Astron. Astrophys. 338, L51–L54 (1998)

ASTRONOMY AND ASTROPHYSICS

LETTER

Letter to the Editor

Properties of the Young Stellar Object N 160 A-IR⋆,⋆⋆

Th. Henning[1], **R. Klein**[1], **S.J. Chan**[2], **E.L. Fitzpatrick**[3], **R. Siebenmorgen**[4], **and B. Stecklum**[5]

[1] Astrophysikalisches Institut und Universitäts-Sternwarte (AIU) Jena, Schillergässchen 2–3, D-07745 Jena, Germany
[2] Institute of Astronomy, University of Cambridge, Madingley Road, Cambridge CB3 0HA, UK
[3] Villanova University, 800 Lancaster Ave., Villanova, PA 19085, USA
[4] ISO Science Operations Centre, Astrophysics Division of ESA, Villafranca del Castillo, P.O. Box 50727, E-28080 Madrid, Spain
[5] Thüringer Landessternwarte Tautenburg, Sternwarte 5, D-07778 Tautenburg, Germany

Received 31 July 1998 / Accepted 20 August 1998

Abstract. We present near- and mid-infrared images of the young stellar object N 160 A-IR in the Large Magellanic Cloud (LMC). For the first time, the YSO is seen in the NIR as a compact point source in the north-western part of the H II region N 160 A. Furthermore, we present ISO-SWS spectra pointed on the YSO. The spectra cover the full wavelength range of SWS on board of ISO (2.5 - 45 μm) where most of the dust features are located. N 160 A-IR shows the unidentified infrared bands (UIBs) and silicate absorption on a steeply rising continuum plus fine structure lines from the H II region. A radiative transfer model for the YSO with a luminosity of $1.4 \cdot 10^6$ $L_\odot$ being deeply embedded (A_V=60 mag) in its parental cloud reproduces the observations. The mass of the model cloud is 50,000 $M_\odot$ consistent with other estimates.

Key words: stars: formation; H II regions; N 160 A; LMC

1. Introduction

The H II region N 160 A is located in a giant molecular cloud (GMC) within the Large Magellanic Cloud (LMC) (Johansson et al. 1998). The GMC is known as the 30 Doradus complex. The cloud complex extends about 3° in north-south direction. To the north of the complex, the most luminous H II region in the Local Group of Galaxies, namely 30 Doradus ≡ N157 (Henize 1956), can be found. South of 30 Doradus is a row of H II regions, namely N 158, N 160, N 159 from the north to the south. It is believed that the star formation process started in 30 Doradus and is now proceeding into the molecular cloud complex and may still go on. South of N 159 is the still quiescent southern part of the GMC (Israel et al. 1996).

Send offprint requests to: R. Klein, rklein@astro.uni-jena.de

⋆ Based on observations with ISO, an ESA project with instruments funded by ESA Member States (especially the PI countries: France, Germany, the Netherlands and the United Kingdom) with the participation of ISAS and NASA.

⋆⋆ Based on observations collected at the European Southern Observatory, La Silla, Chile.

There are two extensive studies of N 160. One study was performed in the optical (Heydari-Malayeri & Testor 1986) and one in the infrared (IR) (Jones et al. 1986). In this work we are only interested in the brightest part, N 160 A. Epchtein et al. (1984; hereafter EBS) found a "protostellar object" (N 160 A-IR) by NIR/MIR photometric observations. With our new NIR/MIR and ISO observations we can confirm the presence and position of the deeply embedded young stellar object (YSO).

2. Observations

In November 1995, J-, H-, K′-band images (central wavelengths λ_0 = 1.24, 1.65, 2.1 μm) of N 160 A were obtained with the IRAC2b camera at ESO's 2.2 m-telescope on La Silla. The presented spectra were observed with the short wavelength spectrometer (SWS) on board the Infrared Space Observatory (ISO) in August 1997. In March 1998, we obtained N-band images (λ_0=10.1 μm) with the MANIAC camera (Böker et al. 1997) at ESO's 2.2 m-telescope clearly showing N 160 A-IR. In addition to these observations, we measured the flux of the dust continuum at 1.3 mm with an on–off observation with the bolometer at the Swedish European Submillimeter Telescope (SEST) on La Silla in March 1995.

2.1. The NIR and MIR images

The K′-band image of N 160 A is displayed in Fig. 1. The small box in Fig. 1 encloses N 160 A-IR. This area is shown enlarged in Fig. 2 for the J-, H-, and K′-band. The designations in Fig. 1 were taken from Jones et al. (1986). The bright objects, N 160 A-9 and N 160 A-5, are identified by Heydari-Malayeri & Testor (1986) as two H II blobs, very dense and highly excited. N 160 A-IR is located in the centre of the small box, easily recognizable by the steeply rising spectral energy distribution (SED) compared to the other objects.

We calibrated the NIR images with the photometric results by Jones et al. (1986). The brightness of N 160 A-IR is

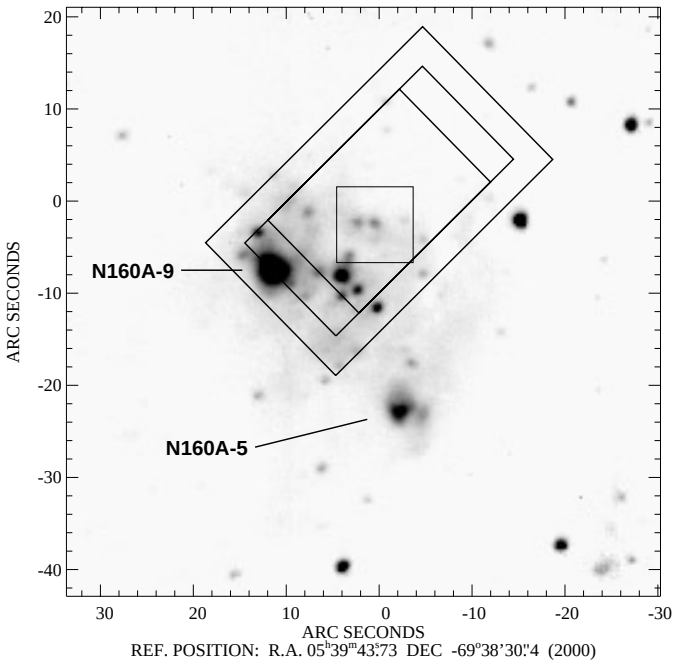

Fig. 1. K′-band image of N 160 A. The three SWS apertures are marked. The small box encloses N 160 A-IR.

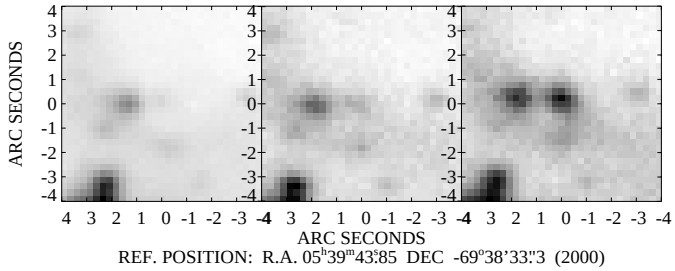

Fig. 2. Enlargement of the area around N 160 A-IR marked with the box in Fig. 1. The YSO is at position (0,0). From the left to the right, the J-, H-, and K′-band images are shown.

14.5±0.2 mag in K′, and upper limits are 16.6 mag in H, and 18.2 mag in J. While the YSO is only a weak object in the K′-band, it is as prominent as the H II blobs at 10 μm indicating its steeply rising SED (Fig. 3). We measured a brightness of 3.14 mag for N 160 A-IR in a 8″ aperture. While the blobs appear still as extended objects, N 160 A-IR is an unresolved point source.

2.2. The SWS spectra

The spectra were observed with the Astronomical Observational Template (AOT) SWS01 with speed 3, i.e. a full scan of the wavelength range of SWS (2.5–45 μm) at a spectral resolution between 250 and 500. The data reduction was done with the interactive analysis software (IA) at the ISO Spectrometer Data Centre in Garching. The spectra shown in Fig. 5 are rebinned to a resolution of 400. They display a continuously rising continuum with several superimposed features. The fine structure lines are marked. These lines are typical for H II regions. We measure a heliocentric velocity of 240 ± 20 km/s for N 160 A using the Doppler-shift of the lines consistent with the velocity of the recombination lines from the H II region of 254 km/s (Whiteoak et al. 1983). The unidentified infrared bands (UIBs) at 6.7, 7.7, 11.3, and 12.7 μm were detected in emission and silicate absorption is seen at 9.7 and at 18 μm. These features are discussed in Sect. 3.

2.3. The millimetre continuum emission

The dust emission at 1.3 mm of N 160 A-IR was measured with an on–off observation with the bolometer at the SEST. We measured 199±14 mJy at the position of the YSO. The beam width of SEST at 1.3 mm is 22″. From the dust emission we can estimate the gas mass of N 160 A-IR. If we assume a dust temperature of 30 K, a dust opacity of 0.4 cm^2/g at 1.3 mm as for the radiative transfer (RT) model (Sect. 3.1), a gas to dust ratio M_g/M_d=300 taking into account the low metallicity of the LMC, and a distance of 50 kpc, we end up with 40,000 $M_\odot$ of gas. Given the uncertainties in the assumptions, this result is uncertain by at least a factor of 4. A gas mass of 60,000 $M_\odot$ was derived by Jones et al. (1986) for the entire N 160 A complex based on FIR data.

3. Discussion

3.1. The protostellar object

EBS reported the detection of "2 new probable protostellar objects in the LMC" by photometric observations. One object was associated with the H II region N 160 A and was called N 160 A-IR. The main reasons for identifying the object as a protostar were the presence of an H_2O maser (Whiteoak et al. 1983), the very steep spectra between 3 and 20 μm, and the silicate absorption feature at 9.7 μm. The multi-aperture photometry performed by EBS resulted in fluxes proportional to the aperture in the bands J, H, and K′. They explained this by a weak contribution of the YSO to the flux which mainly comes from the cloud. NIR imaging by Jones et al. (1986) did not reveal the YSO itself. They associated the eastern blob with N 160 A-IR despite the mismatch in co-ordinates and their J-, H-, K′-band magnitudes.

With our images we can distinguish between the YSO and the surrounding cloud emission. We clearly detect the source in the K′-band on the background of the cloud within the error box for the position given by EBS. The co-ordinates of the source in the K′-band image are RA(2000)=$5^{\rm h}39^{\rm m}43\overset{\rm s}{.}8 \pm 0\overset{\rm s}{.}4$, DEC(2000)=$-69°38'33'' \pm 2''$. There is weak indication for the source in the H-band. We are able to improve the photometry in the NIR by subtracting the cloud contribution. The brightness in the K′- and the upper limits in the J- and H-band are given in Sect. 2.1. Due to its steeply rising SED, N 160 A-IR reaches a brightness comparable to the H II blobs in the N-band.

Fig. 4 compiles the observations of N 160 A together with a SED predicted by a RT calculation (dotted line). Beside the overall shape of the SED, the RT model reproduces the two silicate absorption features quite well. In the spectra the normally strong

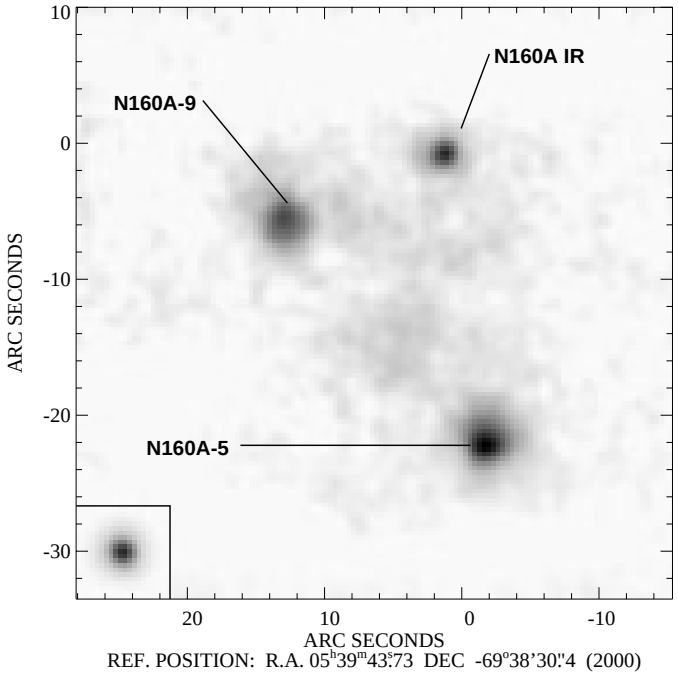

Fig. 3. N-band image of N 160 A. The two H II blobs and the YSO dominate the image. In the small inset the image of α Sco illustrates the point-spread function.

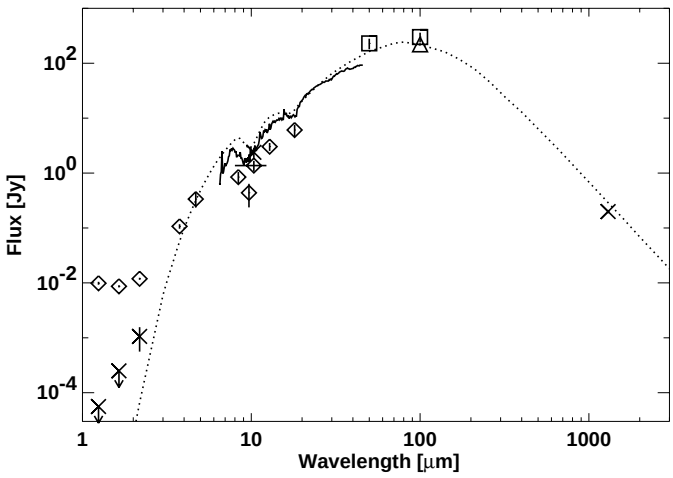

Fig. 4. The spectral energy distribution of N 160 A-IR as observed (diamonds) by EBS, (squares) by Werner et al. (1978), (triangle) by Jones et al. (1986), and (crosses) by us. The dotted line is the SED calculated with a spherically symmetric RT model and the solid line represents the SWS spectra.

silicate feature at 9.7 μm is relatively weak compared to the 18 μm feature but the RT calculation shows the same behaviour and that gives confidence that the low amount of silicates in the dust model and the radial dependence of the density is correct. We used the RT code described by Manske et al. (1998). The dust model consists of carbon (70% by mass; 20% very small grains (VSG) + 50% larger grains) and silicate (30% by mass) particles (spheres) following a size distribution $n(a) \propto a^{-3.5}$. The size of the carbon particles varies from $a = 0.005$ to 1 μm and of the silicate particles from $a = 0.01$ to 1 μm in radius. The very small carbon grains ($a = 0.005$ to 0.1 μm) are treated as transiently heated as described in Manske & Henning (1998). The optical properties for the small carbon grains are taken from Jäger et al. (C400 sample; 1998) and for the larger grains from Draine (1985). For the silicate grains, we took the olivine data by Dorschner et al. (1995). We used a spherically symmetric cloud with a density distribution $\rho \propto r^{-0.3}$ and a radius of 2.6 pc or 10″ at the distance of the LMC. Other power laws ($r^{-0.1...-0.5}$) for the radial dependence would also work with a somewhat different dust composition and total mass. In the centre of the cloud a dust-free cavity with a radius of 300 AU is located. In the cavity we placed an object with a luminosity of $1.4 \cdot 10^6 L_\odot$ and a temperature of 52,500 K, but the result is hardly dependent on the exact value of the temperature. The main parameter of the model is the visual extinction A_V. The observations are reproduced with an A_V=60±10 mag. Assuming again M_g/M_d=300 the cloud mass would be 50,000 $M_\odot$ in good agreement with the estimates discussed in Sect. 2.3.

3.2. The SWS spectra

From the orientation of the SWS slits on the sky it is obvious that different sources contribute to the spectra. The projections of the three SWS apertures on the sky are shown in Fig. 1. The three wavelength ranges (from the smallest to the largest aperture) are: $2\,\mu\text{m} < \lambda_1 < 12\,\mu\text{m}$; $12\,\mu\text{m} < \lambda_2 < 29\,\mu\text{m}$; $29\,\mu\text{m} < \lambda_3 < 45\,\mu\text{m}$. The flux levels of the spectra are almost proportional to the aperture size due to the strong extended emission. Therefore, we scaled the spectra obtained with the smallest and largest aperture with the aperture sizes to match the middle spectrum. Using the N-band image we can estimate the contribution to the continuum of the extended background relative to N 160 A-IR. The background contributes about 60% of the total flux at 10 μm. For spectral features this estimate does not necessarily hold. The fine structure lines may not be intrinsic to N 160 A-IR but may come from all over the H II region as EBS conclude for the Bracket γ line they measured. They find that the Br γ line is not much effected by dust absorption.

The silicate absorption feature was already discussed together with the RT model in Sect. 3.1. Beside the silicate feature, UIBs are also present presumably emitted by polycyclic aromatic hydrocarbon clusters (PAHs). One expects UIBs at 3.3, 6.2, 7.7, 8.6, 11.3, and 12.7 μm. The bands at 3.3 and 6.2 μm were not detected due to noise. We derived an upper limit for the band at 6.2 μm. In addition, we see a feature at 6.7 μm which is not common but is reported e.g. by Gürtler et al. (1996) and Henning et al. (1998). The feature peaking at 7.7 μm has a shoulder on the red side extending up to 8.8 μm. The continuum starts to dominate the spectra at around 10 μm. These spectral features are also seen in compact H II regions in our Galaxy. Roelfsema et al. (1996) have collected six such SWS spectra. The spectral appearance of the UIBs seem to depend on the luminosity of the exciting source. The spectra of the H II regions with highest luminosities are similar to the spectrum of N 160 A-IR, espe-

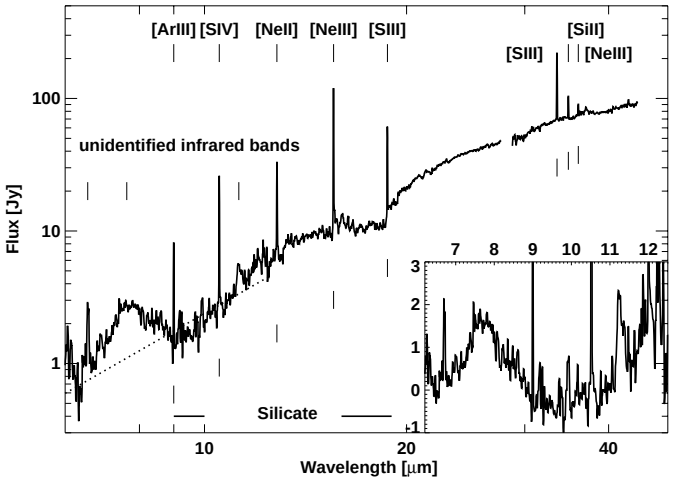

Fig. 5. ISO-SWS spectra of N 160 A. Marked are the detected fine structure lines, UIBs, and the silicate absorption. The spectra are corrected for the different aperture sizes. In the lower left corner the range of the UIBs is displayed in a linear scale. The doted line is subtracted.

Table 1.

Object	6.2/7.7	7.7/8.6	7.7/11.3
N 160 A-IR	$<$0.2	3.3	5.3
IRAS 21190+5140	0.3	7	5

cially the spectrum of IRAS 21190+5140 which have almost the same band ratios (see Table 1). Roelfsema et al. (1996) interpret this dependence with a processing of the PAHs in these high excitation conditions.

It is not that surprising to see silicate and carbon features in the same spectra as the area covered by the SWS apertures encloses different parts of N 160 A. The silicate absorption is produced by the cloud around the YSO and the UIBs may come from the extended emission of the H II region N 160 A.

4. Summary

We reported new observations of the strong infrared source N 160 A-IR detected by EBS. They already identified the object as a YSO based on photometric observations showing a strongly rising SED in the MIR and the presence of an H_2O maser. Our NIR images show, for the first time, the YSO separated from the other bright objects in the H II region N 160 A. The photometry for N 160 A-IR using the NIR images extends the knowledge of the steep SED to shorter wavelengths. NIR and MIR images demonstrate the compact nature of N 160 A-IR. An RT model reproduced the observed SED from the NIR up to millimetre wavelengths. All this is consistent with a deeply embedded YSO (A_V=60 mag) with a luminosity of $1.4 \cdot 10^6 L_\odot$. The mass of the cloud is about 50,000 $M_\odot$ consistent with previous estimates.

Besides the fine structure lines typical of H II regions, the SWS spectra show silicate features in absorption and UIBs in emission. The silicate absorption is relatively weak compared to the total extinction derived from the RT model and is a result of a low silicate abundance in the dust (30%). The observed UIBs are similar to UIBs found in galactic compact H II regions with large luminosities. They are probably coming from polycyclic aromatic hydrocarbon clusters processed in a strong radiation field.

Acknowledgements. We thank M. Feldt and A. Burkert for performing the IR observations, and R. Launhardt for assisting in the SEST observations. R. K. acknowledges support through BMBF-Verbundforschung Astronomie/Astrophysik grant No. 50 OR 9414 9.

References

Böker T., Storey J. W. V., Krabbe A., Lehman T., 1997, PASP 109, 827
Dorschner J., Begemann B., Henning Th., Jäger C., Mutschke H., 1995, A&A 300, 503
Draine B. T., 1985, ApJS 57, 587
Epchtein N., Braz M. A., Sèvre F., 1984, A&A 140, 67
Gürtler J., Henning Th., Kömpe C., et al., 1996, A&A 315, L189
Henize K. G., 1956, ApJ Suppl. 2, 315
Henning Th., Klein R., Launhardt R., Lemke D., Pfau W., 1998, A&A 332, 1035
Heydari-Malayeri M., Testor G., 1986, A&A 162, 180
Israel F. P., Maloney P. R., Geis N., et al., 1996, ApJ 465, 738
Jäger C., Mutschke H., Henning Th., 1998, A&A 332, 291
Johansson L. E. B., Greve A., Booth R. S., et al., 1998, A&A 331, 857
Jones T. J., Hyland A. R., Straw S., et al., 1986, MNRAS 219, 603
Manske V., Henning Th., 1998, A&A, in press
Manske V., Henning Th., Men'shchikov A., 1998, A&A 331, 52
Roelfsema P. R., Cox P., Tielens A. G. G. M., et al., 1996, A&A 315, L289, ISO special issue
Werner M. W., Becklin E. E., Gatley I., et al., 1978, MNRAS 184, 365
Whiteoak J. B., Wellington K. J., Jauncey D. L., et al., 1983, MNRAS 205, 275